Hindawi
Advances in Civil Engineering
Volume 2021, Article ID 2235241, 10 pages
https://doi.org/10.1155/2021/2235241

Research Article

Laboratory Investigation of Fiber Bragg Grating Strain Sensors for Semirigid Base Asphalt Pavements

Jiancun Fu,[1,2] **Aiqin Shen**,[1] **Huaizhi Zhang**,[3] **and Tuanwei Sun**[3]

[1]*School of Highway, Chang'an University, Xi'an Shanxi 710064, China*
[2]*Shandong Transportation Institute, Jinan Shandong 250102, China*
[3]*School of Transportation Engineering, Shenyang Jianzhu University, Shenyang Liaoning 110168, China*

Correspondence should be addressed to Huaizhi Zhang; huaizhi.zhang@163.com

Received 29 July 2021; Revised 26 November 2021; Accepted 7 December 2021; Published 21 December 2021

Academic Editor: Yang Hailu

Aiming to evaluate the applicability of Fiber Bragg Grating (FBG) strain sensors for semirigid pavement monitoring, beam and cylinder specimens with three types of FBG strain sensors embedded in two kinds of classic semirigid pavement materials, asphalt mixture (AC-25) and cement-stabilized crushed stones (CSCS), were prepared in the laboratory. Four-point bending tests and uniaxial-compression tests were carried out under different loading frequencies and temperatures to evaluate the working properties of these sensors and then obtain the corresponding real sensitivity coefficients (SCs). The experimental results showed that the synchronism, repeatability, and linearity of all these sensors were prominent. However, the real SC results were significantly different from the recommended and dependent on many factors including temperature, the loading frequencies, the stress state, and the type of embedded material to different degrees. The SCs remained stable when the moduli of the embedded materials were high enough; otherwise, the SCs varied. Two SC prediction models that used the modulus of the embedded material as the only independent variable were developed to deal with the problem of instability. The modulus difference level between the sensors and the embedded material could integrate the factors roughly, except for the stress state. It is recommended that the factors above should be considered when using FBG strain sensors in practice, and it is still necessary to perform laboratory calibration in advance.

1. Introduction

Monitoring a pavement's internal mechanical responses using sensors embedded in it is a traditional and challenging methodology [1–3]. The measurement results are meaningful to calibrate pavement mechanical-response models, develop new pavement performance-prediction models, control construction quality, develop maintenance policy, and evaluate the application of new structures and materials [2, 4–10]. The measurement accuracy and stability have a decisive influence on the objectives above. Fiber Bragg Grating (FBG) sensors, which have been extensively used in civil engineering in recent years, have significant practical potential in pavements due to the advantages of corrosion resistance, high strength, fatigue resistance, high bandwidth, electric-magnetic resistance, and small size [8, 11–16]. Different types of FBG strain sensors used for asphalt pavement monitoring have been developed, and the limited application sections have revealed exciting prospects [7, 17–25]. However, in the pavement structure, the naked optical FBG is difficult to directly install with the harsh pavement construction and service conditions because of the risk of optical fiber breakage. Therefore, reasonable encapsulation or packaging becomes a necessary process [17, 20, 26–28]. Regardless of the encapsulation form used, there is a multi-stage strain-transfer process when the stress is transmitted, and the problem of strain loss exists [29–31]. Limited laboratory-investigation results have revealed that the accuracy of the strains measured by FBG sensors in the asphalt mixture is highly dependent on the temperature, load characteristics, and embedded material modulus [9, 32]. Numerical analysis has also indicated that the sensors

have a significant disturbance on the stress distribution of the embedded specimen. So, the modulus of the FBG strain sensor should be in an appropriate scope compared to one of the embedded materials, and the sensor length and anchor radius are also important factors influencing measurement accuracy [33, 34]. Based on the above, although the advantages of FBG sensors for pavement monitoring are significant and the practical applications are considerable, the coordinate-deformation ability between sensors and embedded materials is rather complex. Precision modification is still a challenge for this method and needs more consideration.

Therefore, discussing the relationship between the real response and the one measured using FBG sensors is crucial as it determines the credibility of the final monitoring results. In this paper, specific laboratory testing methods were implemented to evaluate the applicability of typical FBG strain sensors in mixtures for semi-rigid base asphalt pavement. The basic performances and sensitive coefficient (SC) variation characteristics of three widely used FBG strain sensors embedded in two typical mixtures were analyzed systematically. The real basic working abilities including synchronization, repeatability, and linearity for the three typical FBG strain sensors embedded in the asphalt concrete and cement-stabilized crushed stones were proved to be prominent through a series of statistical analyses based on the testing results. Whereas the SCs are not always equal to the recommended or stable results and depend on temperature, loading frequency, stress state, and embedded material type of different degree. It is found that the modulus difference level between the sensors and the embedded materials can integrate the factors of temperature, loading frequencies, and embedded material type except stress state and determine the SC stability. Two SC prediction models for the compressing and bending tension states regarding modulus as the independent variable are developed when the SCs are not stable. The key findings above confirm the complexity of the codeformation and reveal the related key factors. The methodology also presents a feasible technical path to gain the accurate SCs. This has the potential to provide help for semirigid base asphalt pavement structure monitoring and enhance the application level of the FBG strain sensors.

2. Materials and Methods

2.1. Basic Parameters of Sensors. The experiments were conducted using three widespread FBG strain sensors in different applications for various pavement measurement purposes, denoted as FBGS-1, FBGS-2, and FBGS-3, as shown in Figure 1. FBGS-1 is designed to measure the vertical strain of some asphalt layer and the length is less than the thickness of most asphalt mixture layer. FBGS-2 and FBGS-3 used to monitor the bending strains should be longer enough to reduce the size effect. Both FBGS-1 and FBGS-2 produced by China Zhixing Science and Technology Nantong Co., Ltd. were encapsulated in fiber-reinforced plastics (FRPs), and FBGS-3 produced by China Geokon Instruments Co., Ltd. was encapsulated in stainless steel. Table 1 lists the key parameters of these three sensors.

2.2. Mixture Design. The asphalt mixture with a 25-mm nominal maximum aggregate (AC-25) that is usually used as the bottom layer of semirigid base asphalt pavement was designed according to the China Technical Specification for Highway Asphalt Pavement Construction (JTGF40-2004), and the mixture of cement-stabilized crushed stones (CSCS) that is a typical semirigid base material was designed according to the China Technical Specification for Construction of Highway Pavement Base Courses (JTG/T F20-2015).

For AC-25, 90# matrix asphalt (PG58-22) was used, the oil-stone ratio was 4.4%, and the gradation curve is listed in Table 2.

For the CSCS mixture, the 425# grade cement content was 4.0%, the optimal water content was 5.3%, the maximum dry density was 2.387 g/cm^3, the average compressive strength for seven days was 4.8 MPa, and the gradation is listed in Table 3.

2.3. Experiment Design and Specimen Preparation. According to the different measuring aims of the three kinds of FBG sensors, the uniaxial-compression test and the four-point bending test were chosen to implement the evaluations, as shown in Figure 2. Specifically, the FBG-1 sensor was designed to be embedded in the middle of the cylindrical specimens, and the FBG-2 and FBG-3 sensors were designed to be embedded at the bottom of the beam specimens. The cylindrical specimens had the compression load *P1* applied from two ends, and the corresponding vertical deformation was recorded with three LVDTs (Linear Variable Differential Transformers) mounted on the side surface. For the beam specimens, two equal forces *P2* were applied on the two inner fourth points, and the corresponding vertical deformation on the top center of the beam was recorded with two LVDTs. The wavelength signals from the FBG sensors were recorded at the sampling frequency of 1000HZ with a fiber grating demodulator model SM130.

In order to meet the embedding requirements of the different sensors, a stainless-steel hollow cylinder with a diameter of 100 mm and a height of 150 mm was specially made with a vertical side groove of 30 mm × 5 mm to accommodate the optical cable. Figure 3 shows the manufacturing process of the cylindrical specimens, which used the static-pressing method. The beam specimens were manufactured through the cutting of rutting testing samples that were compacted by the wheel-rolling method, as shown in Figure 4. For the purpose of accommodating the optical cable, two holes were also drilled on the two-side steel boards of the rutting-sample mold. In order to ensure the adhesion between the sensors and the mixtures, the asphalt or cement paste was painted on the sensor surface before mixture filling. Finally, two cylindrical specimens with the combinations of AC-25 and FBGS-1 as well as CSCS and FBGS-1, along with four beam specimens with the combinations of AC-25 and FBGS-2, CSCS and FBGS-2, AC-25 and FBGS-3, and CSCS and FBGS-3, were successfully prepared, separately.

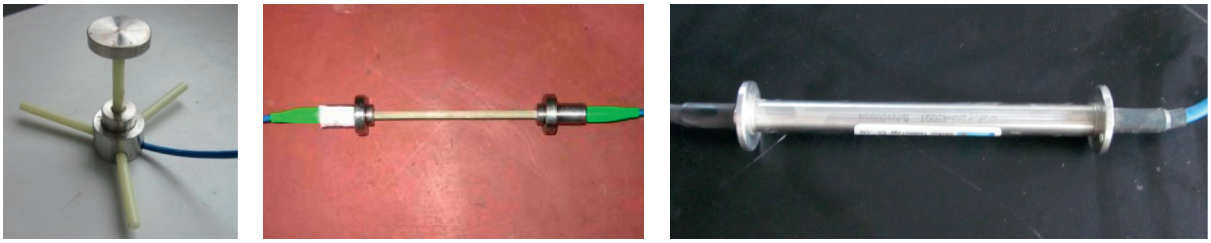

(a) (b) (c)

Figure 1: Three types of FBG sensors.(a)FBGS-1; (b)FBGS-2; (c)FBGS-3.

Table 1: Parameters for the three types of FBG Sensors.

Number	Length (mm)	Package diameter (mm)	Range ($\mu\varepsilon$)	Recommended SC (pm/$\mu\varepsilon$)	Modulus (MPa)
FBGS-1	70	5	±5000	1.2	10000
FBGS-2	140	5	±5000	1.2	10000
FBGS-3	150	12	±1500	0.86	150 (measured direction)

Table 2: AC-25 grading curve.

Screen size (mm)	37.5	31.5	26.5	19.0	16.0	13.2	9.5
Passing percentage (%)	100	99.3	98.6	89.0	73.4	63.9	50.3
Screen size (mm)	4.75	2.36	1.18	0.6	0.3	0.15	0.075
Passing percentage (%)	35.8	23.1	17.0	13.7	9.2	6.9	5.0

Table 3: CSCS gradation curve.

Screen size (mm)	31.5	26.5	19	9.5	4.75	2.36	0.6	0.075
Passing percentage (%)	99.5	93.4	80.7	56.0	39.1	25.6	12.8	6.7

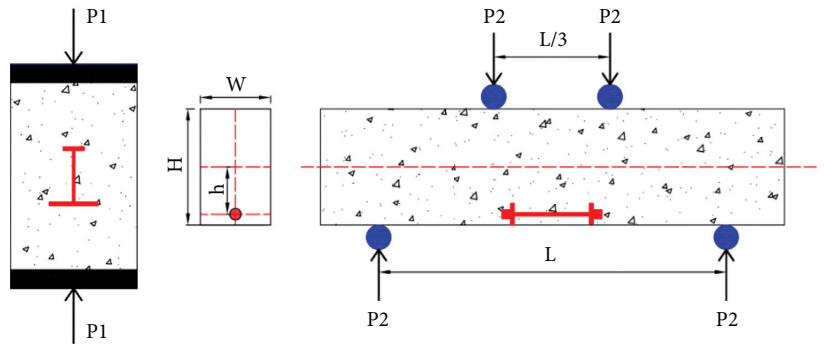

(a) (b)

Figure 2: Schematic diagram of the testing. (a) The uniaxial-compression test; (b) the four-point bending test.

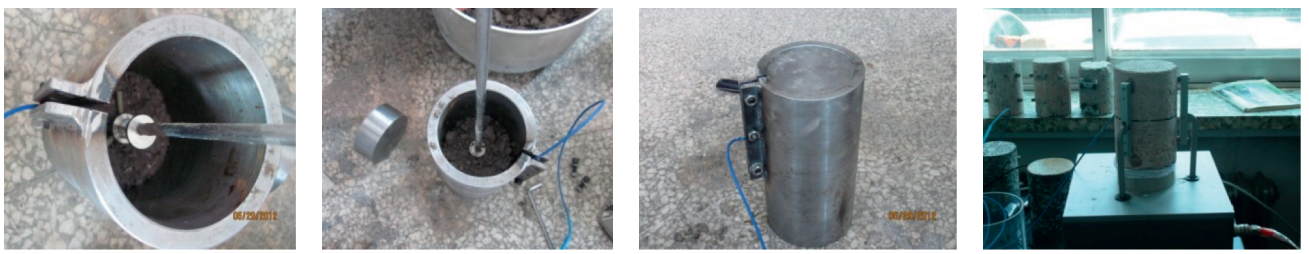

(a) (b) (c) (d)

Figure 3: Cylinder-specimen fabrication procedure. (a) Sensor positioning; (b) mixture filling; (c) after molding; (d) LVDT holder installation.

(a) (b) (c) (d)

Figure 4: Beam-specimen fabrication procedure. (a) Sensor positioning; (b) mixture filling; (c) molding; (d) cutting.

2.4. Experimental Conditions. The testing temperature ranged from −20°C to 30°C, and the specimens were kept at the same temperature for 4 h. Half-sine wave loads with frequencies from 20 to 0.5 Hz were used as the input excitation. A resting time of 10 s was included between any two adjacent frequencies. To maintain the linear viscoelastic or elastic state, for the cylindrical specimens, the maximum applied compressive load *P1* was controlled such that the vertical strain was less than 150 $\mu\varepsilon$. For the beam specimens, the maximum applied load *P2* was controlled such that the bottom bending strain was less than 100 $\mu\varepsilon$. The data of the last five cycles for each frequency were adopted as the basis for the SC determination. The detailed experiment conditions are listed in Table 4.

2.5. Data-Processing Methods. Generally, asphalt mixtures are considered to behave in a linearly viscoelastic manner. Thus, their mechanical response is a continuous function of time and temperature. Consequently, the relationship between the deformation of the asphalt-mixture specimen and time was fitted by the combination of a sine function and a linear function for each testing temperature. The fitting equation was as follows:

$$y = asin(\omega t + \varphi) + bt + c, \tag{1}$$

where y is the fitted variable, a, ω, and φ are the amplitude, angular frequency, and phase angle of the sine function, respectively, t is the time in seconds, and b and c are the slope and intercept of the linear function, respectively.

For the cylindrical specimens, the key indexes including the SC value were calculated using equations (2)–(5):

$$\sigma_c = \frac{\Delta P_c}{\pi r^2}, \tag{2}$$

$$\varepsilon_c = \frac{\Delta D_c}{H_c} \times 10^6, \tag{3}$$

$$E_c = \frac{\sigma_c}{\varepsilon_c} \times 10^6, \tag{4}$$

$$SC_c = \frac{\Delta W}{\varepsilon_c}, \tag{5}$$

where σ_c is the compression-stress amplitude in MPa, ΔP_c is the amplitude of the axial compression load *P1* in MN, r is the radius of the cylindrical specimen in m, ε_c is the compression-strain amplitude in $\mu\varepsilon$, ΔD_c is the vertical deformation amplitude of the cylindrical specimen in mm, H_c is the height of the cylindrical specimen in mm, E_c is the dynamic compression modulus in MPa, SC_c is the sensitivity coefficient of the FBG sensor in the cylindrical specimen in pm/$\mu\varepsilon$, and ΔW is the wavelength amplitude of the FBG sensor in pm.

For the beam specimens, the key indexes including the SC value were calculated using equations (6)–(9):

$$\sigma_b = \frac{Lh\Delta P_b}{WH}, \tag{6}$$

$$\varepsilon_b = \frac{108\Delta D_b h}{23L^2} \times 10^6, \tag{7}$$

$$E_b = \frac{\sigma_b}{\varepsilon_b} \times 10^6, \tag{8}$$

$$SC_b = \frac{\Delta W}{\varepsilon_b}, \tag{9}$$

where σ_b is the tensile-stress amplitude in MPa, L is the beam span in m, h is the position parameter of the FBG sensor in the beam specimen in m, ΔP_b is the amplitude of the bending load P2 in MN, W is the width of the beam specimen in m, ε_b is the bending strain amplitude in $\mu\varepsilon$, E_b is the dynamic bending modulus in MPa, SC_b is the sensitivity coefficient of the FBG sensor in the beam specimen in pm/$\mu\varepsilon$, and ΔW is the same as above.

3. Results

The successful application of sensors in pavement structures depended on two aspects, besides a high survival rate. One was the real-time and stable response performance to the exciting loads, and the other was the accuracy of the measured values. The former focused on the basic performances of the sensor, including the synchronism, repeatability, and linearity, while the latter depended on the SC of the sensor.

3.1. Synchronization. A basic condition of the sensor being applied inside the pavement effectively was that the FBG sensors should respond synchronously with external stimuli. The FBG strain sensor and LVDT signals under the conditions of 20-Hz excitation and 15°C that were obtained

Table 4: Detailed experiment conditions.

Conditions	Values
Temperature (°C)	−20, −10, 5, 15, 30
Loading frequency sequence (hz)	20 (100 cycles), 10 (50 cycles), 5 (20 cycles), 2 (10 cycles), 1 (10 cycles), and 0.5 (10 cycles)

from the test of the beam specimen with the combination of FBGS-2 and AC-25 are shown in Figure 5 as an example due to limited space. The data in Figure 6 were fitted according to Equation (1). The hysteresis of the FBG strain sensor was quantitatively analyzed using the angular frequency ω. The final fitting results were as follows: $\omega_{FBG} = 125.4$ ($R^2 = 0.88$) and $\omega_{LVDT} = 125.5$ ($R^2 = 0.98$). The results showed that the angular frequency of the FBG strain-sensor signal was extremely close to that of the LVDTs, and it was concluded that there was no obvious delay between the two kinds of signals. Therefore, the significant synchronization of the FBG strain sensors was confirmed.

3.2. Repeatability. The repeatability performance of the FBG sensors was also essential for the success of long-term monitoring of pavements. During this experiment, 200 loading cycles were carried out for each specimen under different testing frequencies, as shown in Table 4. As an example, the data of the last five cycles for the specimen with FBGS-2 and AC-25 (0.5 Hz, 15°C) were utilized to evaluate the repeatability performance. The determination coefficients R^2between the signals from the FBG strain sensor and the LVDTs were calculated and compared to evaluate the repeatability quantitatively, as shown in Table 5. It was shown that all R^2 values were greater than 0.95, indicating that there was a strong linear relationship between the FBG strain sensor and the LVDTs. And, consequently, the repeatability of the FBG strain sensors was also prominent.

3.3. Linearity. Linearity is the ability of the FBG sensor installed in the material to maintain a linear reaction under external excitation and is a necessary condition for reasonable monitoring. Good linearity can ensure that the influence of the strain level on the FBG sensor results can be neglected during the calibration process. Figure 6 shows an example of the relationship between the signals of the FBG strain sensor and different strain levels for the specimen with FBGS-1 and AC-25 under the conditions of 10–1 Hz loading frequencies at 15°C. The strain level here refers to the strain amplitude calculated by the data of the LVDTs for the different loading frequencies. The determination coefficient in Figure 6 was 0.996, which means that there was a significant linear characteristic between the FBG sensors and the strain level.

3.4. SC Results. The SCs of all the specimens were calculated according to equations (5) and (9), and the corresponding results are shown in Figure 7.

Based on the results in Figure 7, it is first noted that the calculated SCs were different from the ones recommended by the manufacturers in Table 1. Second, the SCs did not always remain constant. Figures 7(a) and 7(c) show that the SCs had an obvious declining trend with temperature, whereas the others show that the SCs remained at a relatively even level.

To investigate the SC behavior, the possible factors, including temperature, loading frequency, stress state, and embedded material type, influencing the SCs were analyzed as follows.

Temperature had a significant and similar effect for the cylindrical and beam specimens according to Figures 7(a) and 7(c), where FBGS-1 and FBGS-2 with the same FRP package were embedded in the AC-25. The SC trend remained constant at low temperatures and then decreased with the continued increase in temperature. However, the SCs for the other cases remained at a relatively stable level, even when the temperature changed from −20°C to 30°C. Besides, the influence of the loading frequency also existed, as shown in Figures 7(a) and 7(c), when the temperature was more than −10°C, and the SCs for the high loading frequencies were relatively large.

Figures 7(a) and 7(c) along with Figures7(b) and 7(d) were coupled and adopted to compare the influence of the stress state, separately. The FBG sensors in these specimens, FBGS-1 and FBGS-2, had the same parameters, except for the measuring strain direction, as shown in Table 1, and the embedded materials for each couple were also the same. Thus, the measuring strain direction, that is, the stress state, became the only variable. It was found that the SCs in the compression state were significantly different than those in the tension state for the same temperature and loading frequency, although a similar trend existed for each couple.

The influence of the embedded materials on the SCs focused on the difference of the AC25 and the CSCS. Three couples (Figures 7(a)–7(f)) were compared, which were composed of one type of sensor and two types of embedded material. According to Figures 7(a) and 7(b) along with Figure 7(c) and 7(d), the SCs were stable for FBGS-1 and FBGS-2 in the CSCS but varied in the AC-25. However, the SC values for FBGS-3 were always stable for both kinds of embedded material, according to Figures 7(e) and 7(f). Furthermore, the SCs for the same sensor in different embedded materials also varied even though the other factors were the same.

Based on the analysis above in this section, the SC stability was influenced somehow by the temperature, loading frequency, stress state, and type of embedded material. As mentioned in the Introduction, the difference of modulus was the critical factor influencing the co-deformation ability of the sensors. Therefore, the modulus difference between the FBG sensors themselves and the embedded materials was adopted to roughly explain the complex phenomena exhibited by the SC values.

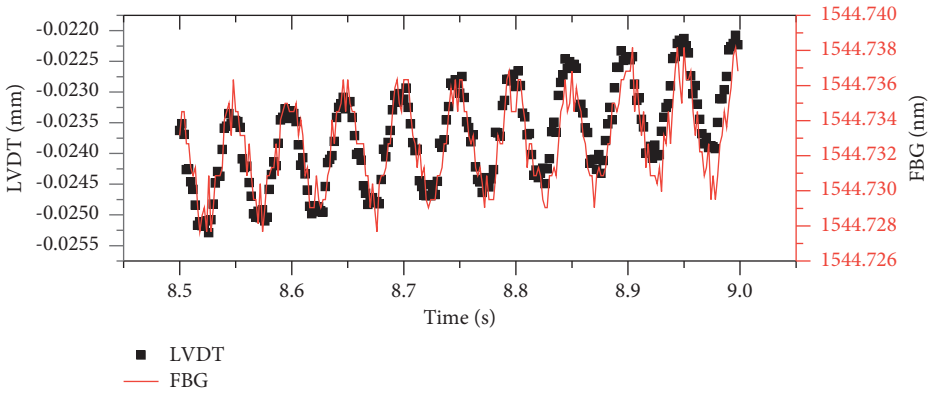

Figure 5: Signal comparison for the LVDTs and the FBG sensor.

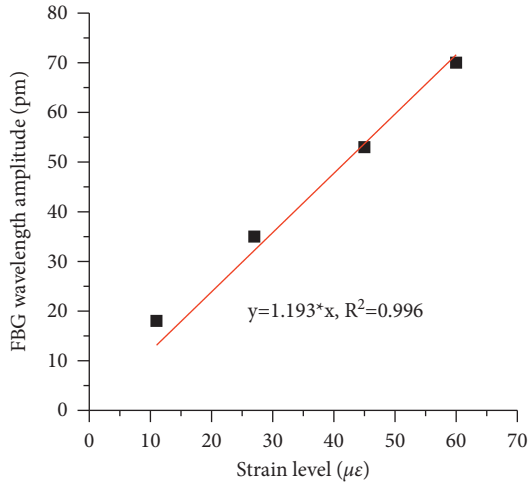

Figure 6: Relationship between the FBG wavelength amplitude and strain level.

Table 5: Determination coefficient R^2 between the FBG sensor and the LVDTs.

Loading cycle sequence of the last five cycles	R^2
1	0.960
2	0.958
3	0.959
4	0.957
5	0.964

The moduli of the CSCS and the AC-25 were calculated according to equations (4) and (8). Both the compression and bending moduli of the CSCS were about 20000 MPa, and the effect of the testing conditions on the moduli was not significant. The compression and bending moduli of the AC-25 ranged from 600 to 20000 MPa and from 5000 to 350000 MPa, respectively, depending on the testing temperature and frequencies. For FBGS-3, the modulus in the measuring direction was 150 MPa, according to Table 1, which was far less than the moduli of the CSCS and AC-25. This implied that FBGS-3 could deform in coordination with the embedded materials. This can be considered as the reason why the SCs for the FBGS-3 always remained stable. For FBGS-1 and FBGS-2, the modulus was 10000 MPa, which was in the range of the AC-25 moduli and in the lower range of the CSCS moduli. This meant that the interaction between the two kinds of sensors and the AC-25 was not negligible when their moduli were comparative. In this case, the deformation of the sensors themselves was less than that of the embedded material because of the relatively large stiffness. As a result, the SCs decreased rapidly as the temperature increased when the moduli of the asphalt mixture AC-25 also decreased quickly, as shown in Figures 7(a) and 7(c).

Based on the analysis above, the SCs and the corresponding modulus data were graphed together in Figure 8 to explore the relationship between the SCs of both FBGS-1 and FBGS-2 and the moduli of the AC-25. As shown in Figure 8, there was a positive correlation between the two variables (the SC and the modulus), and two fitting models with high determination coefficients ($R^2 > 0.94$) were presented. The significant fitting models confirmed the reasonability of explaining the SC variety through the modulus difference and could be used in practice when the modulus is given.

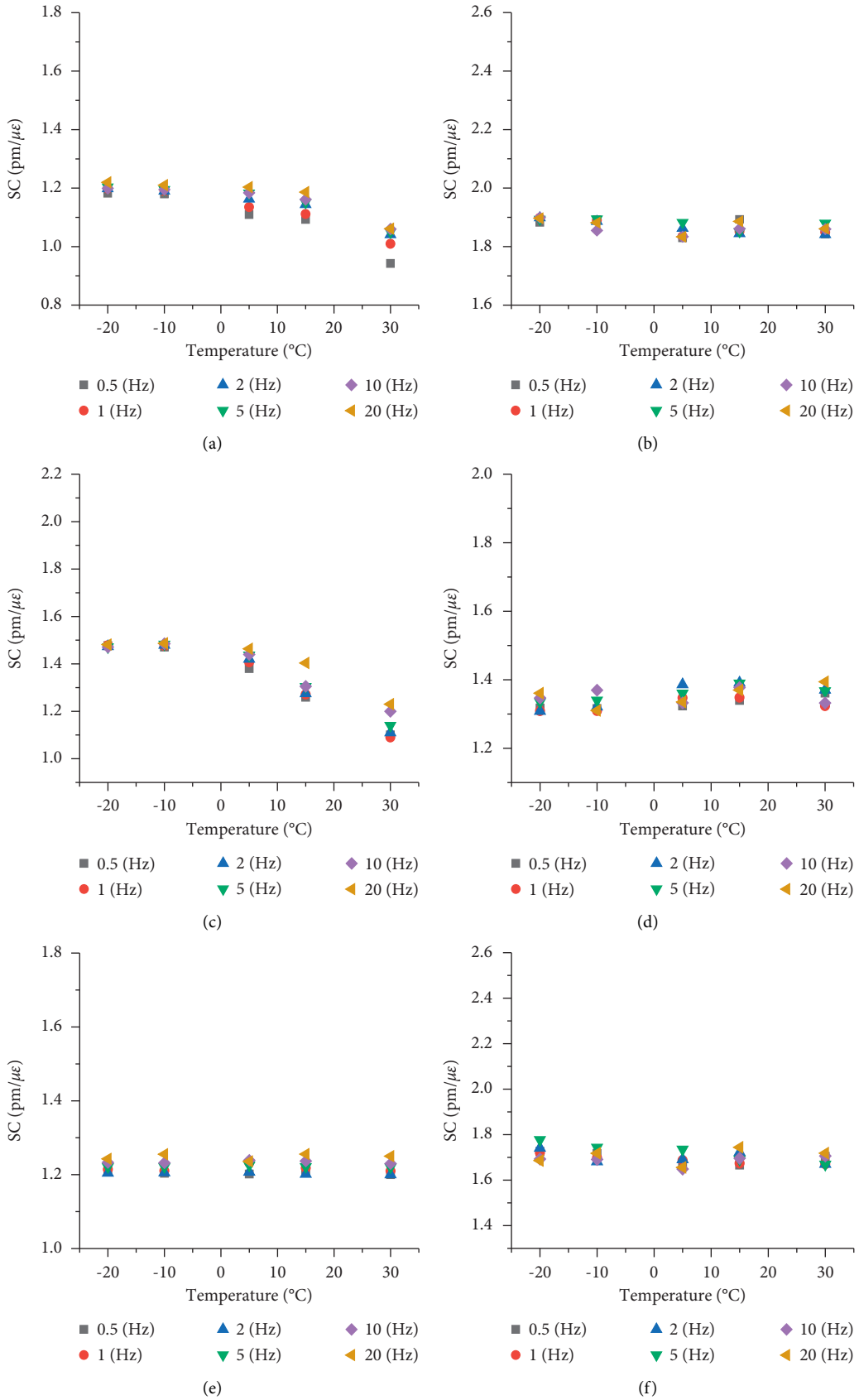

Figure 7: Calculated SC results. (a) FBGS-1 + AC-25; (b) FBGS-1 + CSCS; (c) FBGS-2 + AC-25; (d) FBGS-2 + CSCS; (e) FBGS-3 + AC-25; (f) FBGS-3 + CSCS.

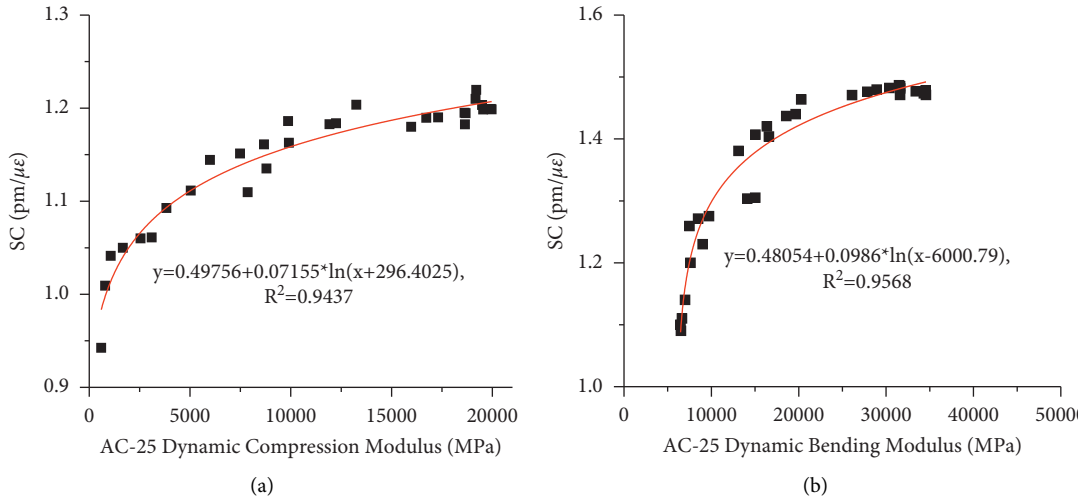

Figure 8: Modulus-based SC prediction model. (a) FBGS-1 + AC-25; (b) FBGS-2 + AC-25.

4. Discussion

Although the benefits of FBG sensors are known, there are still obstacles in the selection of sensors and the confirmation of their monitoring reliability. In this study, to obtain the generality of the results, three widely used FBG strain sensors (FBGS-1, FBGS-2, and FBGS-3), two typical semirigid pavement mixtures (the asphalt concrete AC-25 and the semi-rigid material CSCS), two stress states (the compression and bending tension states), the testing temperature in five groups (−20°C,−10°C, 5°C, 15°C, and 30°C), and six loading frequencies (20 Hz, 10 Hz, 5 Hz, 2 Hz, 1 Hz, and 0. 5 Hz) were considered to cover the situ pavement conditions and monitoring requirements. Firstly, it was shown that the basic performances of synchronization, linearity, and repeatability of the three widely used FBG strain sensors were guaranteed as the necessary conditions of successful monitoring. This means that the three types of FBG sensors could reflect the excitation of the external load linearly in real-time and maintain long-term stability. It was generally believed that the coordinated deformation ability of the sensor itself and the embedded material can be significantly improved by using the methods of end diameter expansion, and the default SCs can be used directly. However, for all three FBG strain sensors, one of the key findings was that the SCs were not the same as those recommended by the manufacturer. Unfortunately, it is common for the recommended SCs of FBG strain sensors to be adopted in a large number of actual applications. Therefore, it was an essential step to investigate the true sensitivity coefficient of the sensor under the actual state and the key factors including the type of the embedded material, loading frequencies, working temperature, and stress state should be considered. In addition, it was found that the SC was sensitive in some special conditions, especially when the modulus of the sensor itself was comparable with that of the embedded material. The modulus difference level could be useful to integrate the factors including temperature, loading frequencies, and embedded material type except stress state to reasonably explain the phenomena of the SCs remaining stable or not. The finding was consistent with some previous research conclusions [33, 34]. Deeper than other studies, the relationship equations with high determination coefficients ($R^2 > 0.94$) between the SCs and the moduli of the embedded material were presented when the SCs were not stable due to different stress state. These two equations can be used to calculate the actual mechanical responses when the FBG sensors and embedded material are the same as those of the situ pavement monitoring and the corresponding temperature and loading frequency are measured to obtain the dynamic modulus of the embedded material in laboratory. Besides, a calibration process that considers the real application conditions for the FBG sensors is necessary according to the analytical results above. The experiment method presented in this study provided a feasible way to obtain the accurate SC values needed to solve the instability problem in practice. Nevertheless, the difference between the calculated SCs and the recommended SCs, even when the SCs are stable, cannot be neglected and still needs further detailed investigation.

5. Conclusions

FBG sensors have significant application potential in pavement monitoring. The mechanism of the interaction and coupling effect between the FBG sensors and the embedded material is not yet clear. Four-point beam bending tests and uniaxial-compression cylinder tests were adopted to investigate the applicability of the three widely used FBG strain sensors in the classic semirigid asphalt-pavement materials, AC-25 and CSCS. The following conclusions were drawn.

The three FBG sensors have excellent basic performances in terms of synchronism, repeatability, and linearity when embedded in the AC25 and CSCS.

In most cases, the calculated SCs from the experimental data are not the same as the manufacturer's recommended values and are affected by the temperature, loading

frequency, stress state, and embedded material type to different degrees. The modulus difference level can roughly explain the direct factors including temperature, loading frequencies, and embedded material type. The SCs remain stable when the moduli of the embedded materials are high enough. Two significant specific fitting models are developed to describe the relationship between the unstable SCs and the moduli of the AC-25.

A laboratory calibration process that considers the real application conditions is necessary for the successful application of FBG strain sensors in semirigid base asphalt-pavement monitoring.

Due to cost limitations, the number of test specimens was insufficient, and more experiments and further research will be carried out in the future work.

Data Availability

Due to the space limitation of the paper, only part of the experimental data is graphed from Sections 3.1 to 3.3 of this paper, but all the data used to support the results of this study can be obtained from the corresponding authors according to the requirements.

Conflicts of Interest

The authors declare no conflicts of interest.

Acknowledgments

This research was supported by the Research and Development Project of Intelligent Assistant Decision System for Pavement Management and Maintenance Design of Shandong Transportation Institute (SDJKY2020-014).

References

[1] M. Barriera, S. Pouget, B. Lebental, and J. V. Rompul, "In situ pavement monitoring: areview," *Infrastructure*, vol. 5, no. 2, p. 18, Article ID 5020018, 2020.

[2] D. Cygas, A. Laurinavitius, and M. Paliukaité, "Monitoring the mechanical and structural behavior of the pavement structure using electronic sensors," *Computer-Aided Civil and Infrastructure Engineering*, vol. 30, no. 4, pp. 317–328, 2015.

[3] L. Sun, H. Zhao, H. Tu, and Y. Tian, "The smart road: practice and concept," *Engineering*, vol. 4, no. 4, pp. 436-437, 2018.

[4] X. Ma, Z. Dong, F. Chen, H. Xiang, C. Cao, and J. Sun, "Airport asphalt pavement health monitoring system for mechanical model updating and distress evaluation under realistic random aircraft loads," *Construction and Building Materials*, vol. 226, pp. 227–237, 2019.

[5] G. Morgan, L. Poulikakos, M. Arraigada, M. Partl, and R. Muff, "In situ monitoring of pavement stresses on the A1 in Switzerland," *Journal of Testing and Evaluation*, vol. 36, no. 4, pp. 291–299, 2008.

[6] L. T. Geng, R. B. Ren, Y. Zhong, and Q. Xu, "Application of FBGsensors in flexible pavement monitoring," *Advanced Materials Research*, vol. 255-260, pp. 3397–3403, 2011.

[7] Z. J. Dong, S. L. Li, J. Y. Wen, and H. C. Chen, "Asphalt pavement structural health monitoring utilizing FBGsensors," *Advanced Engineering Forum*, vol. 5, pp. 339–344, 2012.

[8] P. K. D. Maeijer, G. Luyckx, and C. Vuye, "Fiber optics sensors in asphalt pavement: state-of-the-art review," *Infrastructure*, vol. 4, no. 2, Article ID 4020036, 2019.

[9] J. Xie, H. Li, L. Gao, and M. Liu, "Laboratory investigation of rutting performance for multilayer pavement with fiber Bragg gratings," *Construction and Building Materials*, vol. 154, pp. 331–339, 2017.

[10] Y. Q. Tan, H. P. Wang, S. J. Ma, and H. N. Xu, "Quality control of asphalt pavement compaction using fibre Bragg grating sensing technology," *Construction and Building Materials*, vol. 54, pp. 53–59, 2014.

[11] H.-N. Li, D.-S. Li, and G.-B. Song, "Recent applications of fiber optic sensors to health monitoring in civil engineering," *Engineering Structures*, vol. 26, no. 11, pp. 1647–1657, 2004.

[12] C. K. Y. Leung, K. T. Wan, D. Inaudi et al., "Review: optical fiber sensors for civil engineering applications," *Materials and Structures*, vol. 48, no. 4, pp. 871–906, 2013.

[13] L. Deng and C. S. Cai, "Applications of fiber optic sensors in civil engineering," *Structural Engineering & Mechanics*, vol. 25, no. 5, pp. 577–596, 2007.

[14] J. Lai, J. Qiu, H. Fan et al., "Fiber bragg grating sensors-based in situ monitoring and safety assessment of loess tunnel," *Journal of Sensors*, vol. 2016, pp. 1–10, 2016.

[15] W. R. Habel and K. Krebber, "Fiber-optic sensor applications in civil and geotechnical engineering," *Photonic Sensors*, vol. 1, no. 3, pp. 268–280, 2011.

[16] H. Wang, P. Xiang, and L. Jiang, "Optical fiber sensor based in-field structural performance monitoring of multilayered asphalt pavement," *Journal of Lightwave Technology*, vol. 36, no. 17, pp. 3624–3632, 2018.

[17] R. Scott, M. Vidakovic, S. Chikermane et al., "Encapsulation of fiber optic sensors in 3D printed packages for use in civil engineering applications: apreliminary study," *Sensors*, vol. 19, no. 7, p. 1689, Article ID 19071689, 2019.

[18] C.-Y. Hong, Y.-F. Zhang, M.-X. Zhang, L. M. G. Leung, and L.-Q. Liu, "Application of FBG sensors for geotechnical health monitoring, a review of sensor design, implementation methods and packaging techniques," *Sensors and Actuators A: Physical*, vol. 244, pp. 184–197, 2016.

[19] G. Nosenzo, B. E. Whelan, M. Brunton, D. Kay, and H. Buys, "Continuous monitoring of mining induced strain in a road pavement using fiber Bragg grating sensors," *Photonic Sensors*, vol. 3, no. 2, pp. 144–158, 2012.

[20] Q. L. Hu, C. Wang, and J. P. Ou, "Development and performance research of FBG strain sensor for monitoring on asphalt concrete pavement," *In Sensors and Smart Structures Technologies for Civil, Mechanical, and Aerospace Systems*, vol. 7647, Article ID 847816, 2010.

[21] X. Weng, H.-H. Zhu, J. Chen, D. Liang, B. Shi, and C.-C. Zhang, "Experimental investigation of pavement behavior after embankment widening using a fiber optic sensor network," *Structural Health Monitoring*, vol. 14, no. 1, pp. 46–56, 2014.

[22] M. Imai, Y. Igarashi, M. Shibata, and S. Miura, "Experimental study on strain and deformation monitoring of asphalt structures using embedded fiber optic sensor," *Journal of Civil Structural Health Monitoring*, vol. 4, no. 3, pp. 209–220, 2014.

[23] P. K. D. Maeijer, W. V. D. Bergh, and C. Vuye, "Fiber Bragg grating sensors in three asphalt pavement layers," *Infrastructure*, vol. 3, no. 2, Article ID 3020016, 2018.

[24] J. N. Wang and J. L. Tang, "Using fiber bragg grating sensors to monitor pavement structures. Transportation research record," *Journal of the Transportation Research Board*, vol. 1913, no. 1, pp. 165–176, 2005.

[25] J. Braunfelds, U. Senkans, P. Skels et al., "FBG-based sensing for structural health monitoring of road infrastructure," *Journal of Sensors*, vol. 2021, pp. 1–11, 2021.

[26] H. P. Wang, W. Q. Liu, Z. Zhou, S. Wang, and Y. Li, "The behavior of a novel raw material-encapsulated FBG sensor for pavement monitoring," in *Proceedings of the 2011 International Conference on Optical Instruments and Technology: Optical Sensors and Applications*, Article ID 907211, Beijing, China, November 2011.

[27] Z. Zhang, Y. Huang, L. Palek, and R. Strommen, "Glass fiber-reinforced polymer-packaged fiber Bragg grating sensors for ultra-thin unbonded concrete overlay monitoring," *Structural Health Monitoring*, vol. 14, no. 1, pp. 110–123, 2014.

[28] R. You, L. Ren, and G. Song, "A novel fiber Bragg grating (FBG) soil strain sensorv," *Measurement*, vol. 139, pp. 85–91, 2019.

[29] H. P. Wang and P. Xiang, "Strain transfer analysis of optical fiber based sensors embedded in an asphalt pavement structure," *Measurement Science and Technology*, vol. 27, no. 7, Article ID 075106, 2016.

[30] A. Wang Hua-Ping, B. ZhouZhi, B. Wang Qian, D. Liu Wan-qiu, and F. Jia Ji-han, "Strain transfer errors of optical fiber sensors embedded in asphalt pavement," *Optics and Precision Engineering*, vol. 23, no. 6, pp. 1499–1507, 2015.

[31] H. Wang, P. Xiang, and L. Jiang, "Strain transfer theory of industrialized optical fiber-based sensors in civil engineering: a review on measurement accuracy, design and calibration," *Sensors and Actuators A: Physical*, vol. 285, pp. 414–426, 2019.

[32] Y. Q. Tan, Z. J. Dong, G. L. Tian, and Q. L. Hu, "Evaluating method of the coordination deformation between asphalt mixture and fiber Bragg grating sensor," *Journal of Civil, Architectural & Environmental Engineering*, vol. 31, no. 2, pp. 101–104, 2009.

[33] Z. J. Dong, X. Y. Ma, X. B. Gong, and M. Oeser, "Theoretical evaluation of the measurement accuracy of fiber Bragg grating strain sensors within randomly filled asphalt mixtures based on finite element simulation," *Structural Control and Health Monitoring*, vol. 25, no. 1, p. e2057, 2018.

[34] G. L. Tian, Z. J. Dong, Q. L. Hu, and Y. Q. Tan, "Analysis of coordination between asphalt mixture and fiber Bragg grating sensor," *Journal of Harbin Institute of Technology*, vol. 41, no. 5, pp. 73–76, 2009.